The Journal of Physiology

Relation between activity-induced intracellular sodium transients and ATP dynamics in mouse hippocampal neurons

Niklas J. Gerkau[1], Rodrigo Lerchundi[1], Joel S. E. Nelson[1], Marina Lantermann[1], Jan Meyer[1], Johannes Hirrlinger[2,3] and Christine R. Rose[1]

[1] *Institute of Neurobiology, Faculty of Mathematics and Natural Sciences, Heinrich Heine University Duesseldorf, 40225 Duesseldorf, Germany*
[2] *Carl-Ludwig-Institute for Physiology, University of Leipzig, 04103 Leipzig, Germany*
[3] *Department of Neurogenetics, Max-Planck-Institute for Experimental Medicine, 37075 Goettingen, Germany*

Edited by: Ole Paulsen & Reinhold Penner

Key points

- Employing quantitative Na^+-imaging and Förster resonance energy transfer-based imaging with ATeam1.03^{YEMK} (ATeam), we studied the relation between activity-induced Na^+ influx and intracellular ATP in CA1 pyramidal neurons of the mouse hippocampus.
- Calibration of ATeam *in situ* enabled a quantitative estimate of changes in intracellular ATP concentrations.
- Different paradigms of stimulation that induced global Na^+ influx into the entire neuron resulted in decreases in [ATP] in the range of 0.1–0.6 mM in somata and dendrites, while Na^+ influx that was locally restricted to parts of dendrites did not evoke a detectable change in dendritic [ATP].
- Our data suggest that global Na^+ transients require global cellular activation of the Na^+/K^+-ATPase resulting in a consumption of ATP that transiently overrides its production.
- For recovery from locally restricted Na^+ influx, ATP production as well as fast intracellular diffusion of ATP and Na^+ might prevent a local drop in [ATP].

Niklas J. Gerkau is working as a Post-Doc at the Heinrich Heine University Düsseldorf in the Institute of Neurobiology, Germany. He studied biology in Düsseldorf at the Heinrich Heine University in Germany and obtained his PhD at the Heinrich Heine University Düsseldorf as well. He studied the role of sodium regulation under physiological and pathophysiological conditions in living animals as well as in acute brain slices, employing advanced fluorescence imaging techniques combined with electrophysiological recordings. His current research is focused on early changes in neuronal and astroglial sodium homeostasis during ischaemia in the mouse brain. **Rodrigo Lerchundi** obtained the professional title of Biochemist and a PhD in Science, with mention in Molecular and Cellular Biology, from the Austral University of Chile (UACH, Valdivia, Chile). He worked on his PhD thesis under the tutelage of L. Felipe Barros in the Centre of Scientific Studies (CECs) in Valdivia, Chile. He worked as a Post-Doc at the Institute of Neurobiology at the Heinrich Heine University Duesseldorf, Germany. His work is mainly focused on dynamic ion and metabolite imaging to understand the interaction between neurons and astrocytes under physiological and pathological conditions. **Christine R. Rose** obtained a Diploma in biology from the University of Konstanz and a PhD in Zoology from the Technical University Kaiserslautern (both Germany). She worked as a Post-Doc at the Department of Neurology, Yale School of Medicine (New Haven, CT, USA), and at the Departments of Physiology, Saarland University (Homburg/Germany), the Technical University Munich and the Ludwig Maximilians University Munich (Germany). Since 2005 she has been a full professor and head of the Institute of Neurobiology at the Heinrich Heine University Duesseldorf, Germany. Her work is devoted to cellular ion homeostasis and neuron–glia interaction with a special focus on intracellular sodium homeostasis.

N. J. Gerkau and R. Lerchundi have joint first authorship.

DOI: 10.1113/JP278658

Abstract Excitatory neuronal activity results in the influx of Na^+ through voltage- and ligand-gated channels. Recovery from accompanying increases in intracellular Na^+ concentrations ($[Na^+]_i$) is mainly mediated by the Na^+/K^+-ATPase (NKA) and is one of the major energy-consuming processes in the brain. Here, we analysed the relation between different patterns of activity-induced $[Na^+]_i$ signalling and ATP in mouse hippocampal CA1 pyramidal neurons by Na^+ imaging with sodium-binding benzofurane isophthalate (SBFI) and employing the genetically encoded nanosensor ATeam1.03^{YEMK} (ATeam). *In situ* calibrations demonstrated a sigmoidal dependence of the ATeam Förster resonance energy transfer ratio on the intracellular ATP concentration ($[ATP]_i$) with an apparent K_D of 2.6 mM, indicating its suitability for $[ATP]_i$ measurement. Induction of recurrent network activity resulted in global $[Na^+]_i$ oscillations with amplitudes of ∼10 mM, encompassing somata and dendrites. These were accompanied by a steady decline in $[ATP]_i$ by 0.3–0.4 mM in both compartments. Global $[Na^+]_i$ transients, induced by afferent fibre stimulation or bath application of glutamate, caused delayed, transient decreases in $[ATP]_i$ as well. Brief focal glutamate application that evoked transient *local* Na^+ influx into a dendrite, however, did not result in a measurable reduction in $[ATP]_i$. Our results suggest that ATP consumption by the NKA following global $[Na^+]_i$ transients temporarily overrides its availability, causing a decrease in $[ATP]_i$. Locally restricted Na^+ transients, however, do not result in detectable changes in local $[ATP]_i$, suggesting that ATP production, together with rapid intracellular diffusion of both ATP and Na^+ from and to unstimulated neighbouring regions, counteracts a local energy shortage under these conditions.

(Received 25 July 2019; accepted after revision 23 September 2019; first published online 23 September 2019)
Corresponding author C. R. Rose: Institute of Neurobiology, Faculty of Mathematics and Natural Sciences, Heinrich Heine University Duesseldorf, Universitaetsstrasse 1, D-40225 Duesseldorf, Germany. Email: rose@hhu.de

Introduction

Excitatory electrical signalling of neurons and the generation of action potentials and excitatory postsynaptic potentials mainly relies on the influx of Na^+, which is driven by a large inwardly directed Na^+ gradient. In addition, many other cell functions (e.g. regulation of intracellular Ca^{2+} or pH) are directly or indirectly related to the Na^+ gradient. The Na^+ gradient across neuronal plasma membranes, however, is not stable, but changes under physiological and pathophysiological conditions (Rose, 2002; Somjen, 2004). Indeed, as opposed to the long-held view that electrical signalling does not cause relevant fluctuations in intracellular Na^+ concentrations ($[Na^+]_i$), research over the past years has established that active central neurons experience transient $[Na^+]_i$ elevations. These are predominately caused by Na^+ influx through voltage-gated channels and ionotropic glutamate receptors and are especially prominent in small cellular compartments such as axons and spiny dendrites (Rose & Konnerth, 2001; Miyazaki & Ross, 2017; Ona-Jodar *et al.* 2017).

Recovery from global $[Na^+]_i$ increases is mainly accomplished by the plasma membrane Na^+/K^+-ATPase (NKA), which is the major cellular consumer of ATP (Erecinska & Silver, 1994). NKA exchanges three intracellular Na^+ for two extracellular K^+ (Sweadner, 1995; Kaplan, 2002). Another primary transporter at the plasma membrane is the Ca^{2+}-ATPase, which mediates recovery from activity-induced influx of Ca^{2+} from pre- or postsynaptic compartments (Clapham, 2007). These and other transport processes that maintain ion gradients across the plasma membrane are responsible for most of the brain's energy consumption. Altogether, estimations indicate that ion movements directly related to action potentials require 20–30% of cellular ATP generation, while about 50% is allocated for postsynaptic ion fluxes following synaptic transmission (Lennie, 2003; Howarth *et al.* 2012; Engl & Attwell, 2015).

Despite their considerable need for ATP, neurons lack significant energy stores and are therefore dependent on a constant supply with blood-derived glucose and oxygen to feed their ATP production by mitochondrial respiration and glycolysis. Unsurprisingly, former work established a direct link between cellular energy metabolism, NKA activity and Na^+ regulation, demonstrating that metabolic failure results both in large shifts in neuronal $[Na^+]_i$ and a substantial decrease in intracellular ATP concentrations ($[ATP]_i$) with secondary breakdown of other ion gradients and detrimental consequences (Hansen, 1985; Erecinska & Silver, 1994; Leng *et al.* 2014; Gerkau *et al.* 2017). In addition to ATP-dependent ion transporters, many neurons express K_{ATP} channels that couple their metabolic state to their excitability and which are activated by a more moderate decline in cellular [ATP] (Proks & Ashcroft, 2009; Tanner *et al.* 2011; Mollajew *et al.* 2013; Martinez-Francois *et al.* 2018).

The conditions under which excitatory activity and accompanying Na^+ influx may actually affect levels of ATP or other metabolites in neurons in the brain are, at present, only partly understood. To answer these questions and gain more insight into brain metabolism, protein-based, genetically encoded fluorescent indicators are increasingly employed (Tantama *et al.* 2012). Here, we have used the Förster resonance energy transfer (FRET)-based nanosensor ATeam1.03^{YEMK} (ATeam) (Imamura *et al.* 2009), which has already been successfully employed to analyse ATP dynamics in neurons and astrocytes in cell culture and in brain tissue (Trevisiol *et al.* 2017; Winkler *et al.* 2017; Baeza-Lehnert *et al.* 2019; Lerchundi *et al.* 2019). Using this tool, we studied the relationship between different patterns of activity, Na^+ transients and [ATP] in somata and dendrites of CA1 pyramidal neurons in mouse hippocampal tissue slices. In our study, we also provide the first calibration of ATeam inside neurons, suggesting that this sensor is suitable to detect changes in neuronal [ATP].

Methods

Ethical approval

The present study was carried out in strict accordance with the institutional guidelines of the Heinrich Heine University Düsseldorf as well as the European Community Council Directive (2010/63/EU). All experiments using brain slices were communicated to and approved by the Animal Welfare Office at the Animal Care and Use Facility of the Heinrich Heine University Düsseldorf (institutional act no. O50/05). In accordance with the recommendations of the European Commission (Close *et al.* 1997), animals up to 10 days old were killed by decapitation, while older mice were anaesthetized with CO_2 and then quickly decapitated.

Preparation of acute brain slices and organotypic tissue slice cultures

Brain tissue slices were prepared from hippocampi of Balb/C mice (postnatal day (P) 6–8 or 14–20; both sexes). Moreover, transgenic mice (P21–25; both sexes) expressing the ATP-sensor ATeam (Imamura *et al.* 2009) under the murine *Thy1.2* promoter were used (B6-Tg(Thy1.2-ATeam1.03^{YEMK})AJhi; MGI:5882597; Trevisiol *et al.* 2017). For generation of acute hippocampal tissue slices, animals were anaesthetized, decapitated and their brains quickly removed. Brains were immediately placed in ice-cold preparation saline, containing (in mM): 125 NaCl, 2.5 KCl, 0.5 $CaCl_2$, 6 $MgCl_2$, 1.25 NaH_2PO_4, 26 $NaHCO_3$, and 20 glucose, bubbled with 95% O_2/5% CO_2, resulting in a pH of 7.4 and an osmolarity of 310 ± 5 mOsm l^{-1}. Subsequently, brains were separated into hemispheres and cut into 250 µm-thick slices in a parasagittal orientation using a vibrating blade microtome (HM 650 V; Thermo Fisher Scientific, Waltham, MA, USA).

After cutting, slices were incubated at 34°C for 30 min in artificial cerebrospinal fluid (ACSF), containing (in mM): 125 NaCl, 2.5 KCl, 2 $CaCl_2$, 1 $MgCl_2$, 1.25 NaH_2PO_4, 26 $NaHCO_3$, and 20 glucose, bubbled with 95% O_2/5% CO_2, resulting in a pH of 7.4 and an osmolarity of 310 ± 5 mOsm l^{-1}. Subsequently, slices were kept in ACSF at room temperature (20–22°C) and used for up to 6 h. Experiments were performed at room temperature as well.

Organotypic hippocampal tissue slice cultures were prepared following a protocol by Stoppini *et al.* (1991). Briefly, tissue slices were obtained from P6–P8 mice under sterile conditions and immediately transferred onto Biopore membranes (Millicell standing insert, Merck Millipore, Burlington, MA, USA). They were then kept in an incubator at 36.5°C for at least 10 days at an interface between humidified carbogen (95% O_2/5% CO_2) and culture medium (Gee *et al.* 2017) containing minimum essential medium (MEM; M7278; Sigma-Aldrich, Munich, Germany), 20% heat-inactivated horse serum (Origin, Brazil; Thermo Fisher Scientific, USA), 1 mM L-glutamine, 0.01 mg ml^{-1} insulin, 14.5 mM NaCl, 2 mM $MgSO_4$, 1.44 mM $CaCl_2$, 0.00125% ascorbic acid and 13 mM D-glucose. The medium was replaced every 3 days and organotypic slices were used for experiments between 10 and 21 days in culture.

To induce disinhibition and recurrent network activity, slices were perfused with a saline nominally devoid of Mg^{2+}, to which the $GABA_A$ receptor blocker bicuculline was added at a concentration of 10 µM. Electrical stimulation of Schaffer collaterals was performed using a glass micropipette filled with HEPES-buffered saline. The pipette was positioned into the stratum radiatum at a distance of 100–150 µm from the cells of interest and a train of stimuli (10 pulses at 50 Hz) was delivered using a stimulus generator (Isolated Stimulus Generator Model 2100, A-M Systems, Carlsborg, WA, USA). Bath application of glutamate was performed by perfusing the slices with ACSF to which 1 mM glutamate was added. For focal pressure application onto dendrites, glutamate was dissolved at 1 mM in Hepes-buffered saline composed of (in mM): 125 NaCl, 2.5 KCl, 2 $CaCl_2$, 2 $MgCl_2$, 1.25 NaH_2PO_4 and 25 HEPES, pH 7.4 (adjusted with NaOH). This solution was filled into a fine-tipped glass pipette and delivered using a pressure application system (PDES nxh, npi electronic, Tamm, Germany).

All chemicals were purchased from Sigma-Aldrich (Munich, Germany), unless otherwise noted. β-Escin for permeabilization of plasma membranes was obtained from mpbio (Illkirch, France).

Field potential recordings and determination of extracellular sodium

Field potential recordings were performed at 1 kHz in the stratum radiatum of the CA1 region using sharp glass microelectrodes filled with ACSF coupled to an Axopatch 200B amplifier and a Digidata 1322A (Molecular Devices, Sunnyvale, CA, USA). Data traces were filtered using a Savitzky-Golay filter and analysed with OriginPro 8.5G software (OriginLab Corp., Northhampton, MA, USA).

Extracellular Na^+ concentrations ($[Na^+]_o$) were determined using concentric, Na^+-sensitive microelectrodes as described earlier (Haack *et al.* 2015). Briefly, Na^+-sensitive microelectrodes were prepared from thin-walled borosilicate glass capillaries with filament. The Na^+-sensitive capillary was filled with liquid neutral ion carrier based on ETH 157 (Ionophore II, Cocktail A, Fluka, Buchs, Switzerland). The reference electrode was filled with HEPES-buffered saline. Electrodes were positioned ∼50 µm below the slice surface into the CA1 stratum radiatum. They were calibrated in the experimental bath directly before and after each individual experiment using HEPES-buffered saline containing defined sodium concentrations ($[Na^+]$) ranging from 70–160 mM (with Na^+ replaced by *N*-methyl-D-glucamine chloride (NMDG-Cl) to maintain iso-osmolarity).

Sodium imaging

For imaging of $[Na^+]_i$ in CA1 pyramidal neurons, the membrane-permeant form of SBFI (SBFI-AM; 200 µM, Teflabs, Austin, TX, USA) was pressure-injected into the stratum radiatum and stratum oriens as reported before (Meier *et al.* 2006; Langer *et al.* 2017). Alternatively, individual CA1 neurons were subjected to whole-cell patch-clamp and loaded with the membrane-impermeant salt of SBFI (Teflabs) through the patch pipette for at least 15 min before starting imaging experiments. The pipette solution contained (in mM): 145 $KMeSO_3$, 40 KCl, 12.5 Hepes, 10 NaCl, 5 Mg-ATP, 0.5 Na_3-GTP, and 1 SBFI; pH was adjusted to 7.3. Neurons were held in the voltage-clamp mode at −70 mV (liquid junction potential not corrected) using an EPC10 amplifier (HEKA Elektronik, Lambrecht, Germany) and PatchMaster software (HEKA Elektronik). In some experiments, the patch pipette was carefully retracted after sufficient dye-loading of fine dendrites and Na^+ imaging was commenced after ∼15 min to allow re-sealing of the cell membrane.

Multiphoton imaging of SBFI was performed employing a custom-build laser-scanning system based on a FluoView300 (Olympus Europe, Hamburg, Germany) coupled to a femtosecond-pulsed infrared laser (MaiTai; Spectra Physics, Darmstadt, Germany), equipped with a water immersion objective (NIR Apo ×60/NA 1.0, Nikon Instruments Europe, Düsseldorf, Germany). Excitation wavelength was 800 nm, fluorescence emission was collected <700 nm. Images were acquired at 1–5 Hz and fluorescence emission from selected regions of interest (ROIs) was analysed offline using FluoView 5.0 (Olympus Europe) and OriginPro software. After each experiment, Z-stacks were generated at a step size of 1 µm for reconstruction of entire cells and at 0.2 µm for reconstruction of dendrites. Images were post-processed employing deconvolution software to delineate cellular morphology (Huygens Professional, SVI imaging, Hilversum, Netherlands).

SBFI fluorescence was calibrated *in situ* as described previously (Rose *et al.* 1999; Meier *et al.* 2006; Gerkau *et al.* 2018). Briefly, SBFI-AM-loaded organotypic tissue slices were first superfused with nominally Na^+-free calibration-ACSF, containing ouabain (100 µM), an inhibitor of the Na^+/K^+-ATPase, as well as the ionophores gramicidin (3 µM) and monensin (10 µM) to equilibrate intra- and extracellular Na^+. Afterwards, slices were exposed to calibration-ACSFs containing different $[Na^+]$ and resulting changes in SBFI fluorescence in neuronal somata were recorded using multiphoton excitation. As reported before (Rose *et al.* 1999; Meier *et al.* 2006; Gerkau *et al.* 2018), increasing $[Na^+]$ caused a decrease in fluorescence emission of SBFI and traces were inverted for illustration purposes after normalization to fluorescence levels at 0 mM (Fig. 1*A*). Normalized changes in SBFI fluorescence were plotted against $[Na^+]$ and fit using Michaelis–Menten kinetics (Fig. 1*B*).

Determination of intracellular ATP

For expression of the genetically encoded sensor ATeam (Imamura *et al.* 2009) in cultured organotypic slices, an adeno-associated viral vector (AAV2/5) containing the sequence of the sensor under the human-synapsin1 promoter (packaged by the Viral Vector Facility of the University/ETH Zürich, Switzerland) was employed as described previously (Lerchundi *et al.* 2019*b*). Briefly, 0.5 µl of the vector (virus titre: 1.375×10^{12} viral genome ml^{-1}) was directly applied on top of slices at 1–3 days *in vitro*, and then kept in culture for at least 7 more days before use. Alternatively, for imaging of ATP levels in acute tissue slices, transgenic mice expressing ATeam under the murine *Thy1.2* promoter were used (Trevisiol *et al.* 2017).

ATP imaging was performed employing a wide-field fluorescence microscope (Nikon Eclipse FN-I, Nikon GmbH Europe) equipped with a lambda DG-4 illumination unit (Sutter Instrument Co., Novato, CA, USA) and a variable scan digital imaging system (Nikon NIS-Elements v4.3, Nikon GmbH Europe). Moreover, a water immersion objective (×40/NA 0.8 LUMPlanFI; Olympus Deutschland GmbH, Hamburg, Germany)

and an Orca Flash V2 camera (Hamamatsu Photonics Deutschland GmbH, Herrsching, Germany) were used. ATeam was excited at 434 nm (434/17 nm) and the emitted fluorescent light was split at 500 nm with a W-VIEW GEMINI A12801-01 optic system (Hamamatsu Photonics Deutschland GmbH), equipped with band pass filters at 483/32 (enhanced cyan fluorescent protein; eCFP) and 542/27 nm (Venus) (Fig. 1*C*).

Fluorescence emission was detected from cellular ROIs expressing the sensor using NIS-Elements software (Nikon GmbH Europe). For background correction, a region of interest (ROI) in the field of view apparently devoid of cellular structures expressing the sensor was chosen and its signals subtracted from those derived from defined cellular ROIs. The ΔATeam ratio was calculated by dividing the fluorescence emission of Venus (FRET acceptor) by the eCFP fluorescence (FRET donor) and normalizing it to the baseline under control conditions (Fig. 1*D*).

Changes in the ΔATeam ratio were converted into changes in intracellular [ATP] based on a calibration

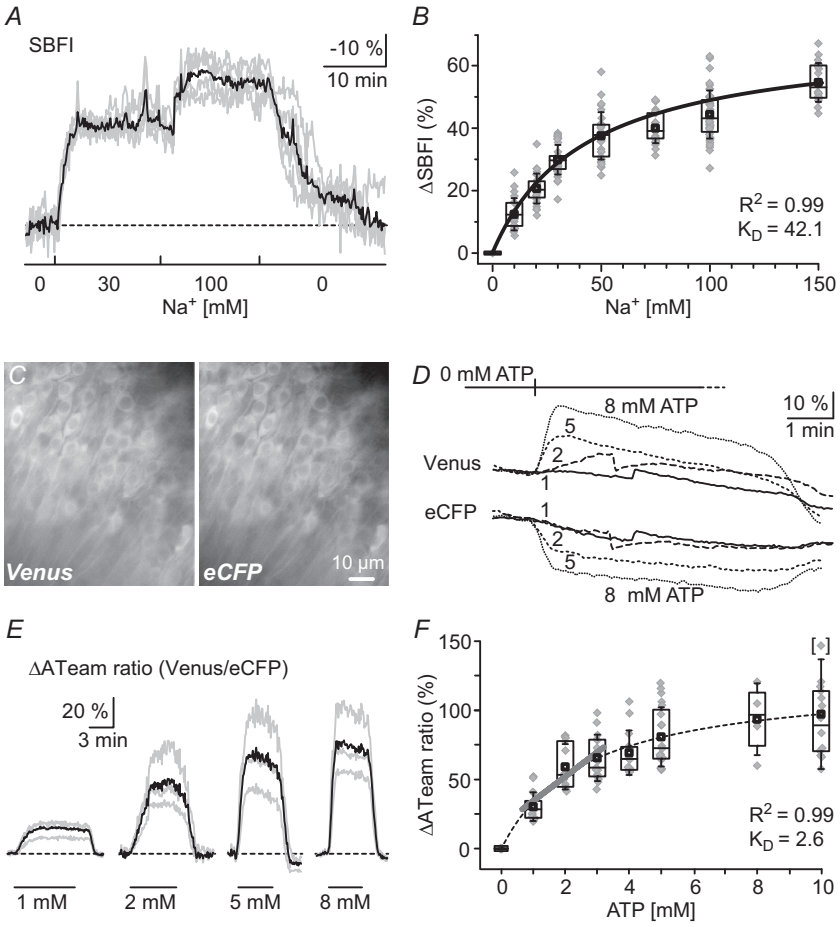

Figure 1. Calibration of SBFI and ATeam1.03^{YEMK} in pyramidal neurons
A, relative changes in cellular SBFI fluorescence (evoked by multiphoton excitation at 800 nm) in an organotypic slice in the presence of Na^+ ionophores upon changing [Na^+] as indicated, normalized to fluorescence at 0 mM Na^+. *B*, plot of normalized changes in SBFI fluorescence *vs.* [Na^+]. The line represents a Michaelis–Menten fit of the data, revealing an apparent K_D of 42.1 mM. *C*, images of Venus (left) and eCFP (right) fluorescence of CA1 pyramidal neurons in an organotypic slice expressing ATeam, taken with a wide-field fluorescence microscope. *D*, changes in Venus and eCFP fluorescence in neurons expressing ATeam during a calibration in response to changes in [ATP] from 0 to 1, 2, 5, or 8 mM as indicated. In the traces showing changes to 1 and 2 mM ATP in Venus and eCFP, movement artifacts were generated due to re-focusing. *E*, resulting change in the ΔATeam ratio. Note that the movement artifacts at 1 and 2 mM ATP in *D* are cancelled out by calculating the ratio. *F*, plot of normalized changes in ΔATeam ratio *vs.* [ATP]. The data point in brackets is an outlier at 10 mM ATP (213.5%). The dashed line represents a Michaelis–Menten fit of the data, revealing an apparent K_D of 2.6 mM. The thick grey line represents a linear fit of the data between 1 and 3 mM ATP. *A* and *E*: grey lines represent traces from individual somata and the black line represents the averaged response. *B* and *F* show means (black squares), IQR (box), median (line), SD (whiskers) and all single data points (grey diamonds).

procedure performed in organotypic slice preparations as described in the Results section. To mimic intracellular ion composition, a saline composed of 25 mM NaCl, 129 mM potassium gluconate, 10 mM HEPES and 10 mM $MgCl_2$, titrated to pH 7.3, was used during these calibrations.

Data analysis and statistics

Unless otherwise specified, data are presented in Tukey box-and-whisker plots indicating median (line), mean (square), interquartile range (IQR; box) and standard deviation (whiskers). In addition, all individual data points are shown in grey underneath the Tukey plots. Data were statistically analysed by either Student's *t*-test or one-way ANOVA followed by *post hoc* Bonferoni test. The following symbols are used to illustrate the results of statistical tests in the figures: *: $0.01 \leq P < 0.05$; **: $0.001 \leq P < 0.01$; ***: $P < 0.001$. *n* represents the number of cells or individual dendrites analysed; *N* represents the number of individual experiments/slice preparations. Each series of experiments was performed on at least three different animals.

Results

Quantitative determination of $[Na^+]$ and [ATP] in neurons

The goal of the present study was to analyse the relation between changes in $[Na^+]_i$ and $[ATP]_i$ evoked by different patterns of activity in principal neurons. To this end, we employed quantitative multi-photon Na^+ imaging with the fluorescent dye SBFI in CA1 pyramidal neurons of mouse hippocampus. Calibration of SBFI fluorescence was performed in CA1 neurons of organotypic slice culture ($n = 20$–46 individual cells and $N = 3$ tissue slices for each $[Na^+]$ tested; see Fig. 1*A*) and followed established procedures as described in detail previously (Rose *et al.* 1999; Meier *et al.* 2006; Ona-Jodar *et al.* 2017). The relation between normalized changes in SBFI fluorescence and $[Na^+]$ followed Michaelis–Menten kinetics, revealing an apparent K_D of 42.1 mM (Fig. 1*B*). A baseline $[Na^+]_i$ of 10 mM, corresponding to the $[Na^+]$ of the intracellular saline, was assumed for cells held in whole-cell patch-clamp. For neurons in bolus-loaded slices, we assumed a baseline $[Na^+]_i$ of 13.4 mM according to our earlier study (Mondragao *et al.* 2016). Based on these parameters and the *in situ* calibration, changes in SBFI fluorescence observed upon different pattern of stimulations were normalized to baseline levels and converted into changes in $[Na^+]_i$ in the following.

For measurement of $[ATP]_i$ in CA1 pyramidal neurons, we employed the genetically encoded sensor ATeam (Imamura *et al.* 2009). While in former work (e.g. Trevisiol *et al.* 2017; Winkler *et al.* 2017; Lerchundi *et al.* 2019*b*), ATeam was employed to monitor relative changes in cellular ATP levels, we aimed to establish a more quantitative approach by performing an intracellular calibration. To this end, ATeam was expressed under the human-synapsin1 promoter in organotypic tissue slices. As reported before (Lerchundi *et al.* 2019*a*,*b*), this resulted in a specific transduction and expression of ATeam in neurons. Cell bodies of individual CA1 pyramidal neurons and adjacent primary dendrites could be distinguished based on the fluorescence emission of the donor (eCFP) and the acceptor (Venus) (Fig. 1*C*). Their normalized ratio (ΔATeam ratio) was then calculated as described below to reveal changes in cellular ATP following a procedure introduced previously (Fig. 1*D* and *E*) (Lerchundi *et al.* 2019*b*).

For calibration of ATeam, cultured slices expressing the sensor were first superfused with a saline containing 50 μM *β*-escin, a saponin which induces pore formation and permeabilization of plasma membranes in a dose-dependent manner (Konishi & Watanabe, 1995; Akagi *et al.* 1999). Subsequently, slices were exposed to ATP-free saline containing low $[Na^+]$ and high $[K^+]$ to mimic intracellular concentrations of these major cations. In addition, this saline contained NaN_3 (5 mM; an inhibitor of the mitochondrial complex IV), 2-deoxy-D-glucose (2-DG, 2 mM; a non-metabolizable glucose analogue) and Na_3VO_4 (0.1 mM; a non-selective ATPase inhibitor) to minimize the cellular production and consumption of ATP. Afterwards, defined concentrations of ATP ranging from 1 to 10 mM were added to the nominally ATP-free saline. Changes in Venus and eCFP fluorescence were recorded from cell bodies of CA1 pyramidal neurons and converted into changes in the ATeam ratio ($n = 14$–20 individual cells and $N = 3$–5 tissue slices for each ATP concentration tested; see Fig. 1*D* and *E*). These were normalized to the ATeam ratio at 0 mM ATP, and the resulting ΔATeam ratio values plotted against the [ATP], after which data were fit with a Michaelis–Menten function, revealing an apparent K_D of 2.63 mM (Fig. 1*F*).

Addition of *β*-escin and exposure to calibration salines caused a swelling of neurons and resulted in tissue movement and changes in focus. The required re-focusing prevented a reliable deduction of cellular baseline [ATP] in individual cells from these calibrations. Based on earlier studies, which determined baseline [ATP] of ∼2 mM in different neurons (Fukuda *et al.* 1983; Ainscow *et al.* 2002; Mollajew *et al.* 2013; Rangaraju *et al.* 2014; Toloe *et al.* 2014; Pathak *et al.* 2015), data derived from calibrations were fit linearly for [ATP] between 1 and 3 mM ($R^2 = 0.76$) (Fig. 1*F*). Of note, for decreases in [ATP] by a maximum of 0.5–0.6 mM as detected in the present study (see below), this linearization is applicable for baseline ATP levels between ∼1.5 and 3 mM. This enabled a conversion of the ATeam signals into changes in [ATP] in the following,

with a 10% change in the ΔATeam ratio corresponding to a change in [ATP] by 0.57 mM.

Taken together, these results confirm that SBFI is a suitable dye for the imaging of activity-related changes in $[Na^+]_i$ as established before. In addition, our data demonstrate that ATeam can be calibrated *in situ* and, when expressed in pyramidal neurons, exhibits an apparent K_D of 2.6 mM for ATP. This implies that ATeam can be employed for quantitative imaging of changes in neuronal [ATP].

Network $[Na^+]$ oscillations induce a decrease in neuronal [ATP]

To study if activity-related changes in neuronal $[Na^+]_i$ are accompanied by changes in intracellular [ATP] in our preparation, we first employed an established paradigm for induction of recurrent network activity. To this end, acute hippocampal slices were perfused with nominally Mg^{2+}-free saline containing 10 μM bicuculline methiodide ($0Mg^{2+}$/BIC) to unblock NMDA receptors and reduce inhibition by $GABA_A$ receptors. As reported before (Karus *et al.* 2015), this resulted in regular changes in the field potential recorded from the stratum radiatum, indicating burst activity of the neuronal network within a few minutes upon perfusion with $0Mg^{2+}$/BIC saline ($N = 5$) (Fig. 2*A*). Large epileptiform bursts lasted ∼5 s, hosted several population spikes and occurred at a frequency of 1–2 per minute. In between, smaller and shorter biphasic events occurred every ∼20 s (Fig. 2*A*).

Regular electrical bursting activity was accompanied by rapid transient dips in the extracellular $[Na^+]$ ($[Na^+]_e$) in the stratum radiatum as determined using concentric Na^+-sensitive microelectrodes. These averaged 2.2 ± 0.7 mM in the time window between 10 and 15 min after starting the perfusion with $0Mg^{2+}$/BIC (range: 1.0–4.5 mM; median: 2.1 mM; $n = 46$ signals, $N = 5$) (Fig. 2*B*). Moreover, apparent baseline $[Na^+]_e$ steadily decreased by about 3 mM during a 30 min exposure to $0Mg^{2+}$/BIC saline (Fig. 2*B*). The slow decrease in $[Na^+]_e$ essentially mirrored the slow and steady increase in neuronal $[Na^+]_i$ by ∼2 mM reported to occur under these conditions (Karus *et al.* 2015).

For Na^+ imaging in somata of CA1 pyramidal cells, slices were bolus-loaded with SBFI-AM (Fig. 1*C*). This revealed that essentially the entire neuronal population in the pyramidal layer showed regular transient increases in $[Na^+]_i$ in the presence of $0Mg^{2+}$/BIC (Fig. 2*C*), termed 'network Na^+ oscillations' in our earlier work (Karus *et al.* 2015). Their peak amplitudes amounted to 9.8 ± 3.7 mM in cell bodies (range: 3.0–22.4 mM; median: 9.5 mM; $n = 239$ cells, $N = 4$) (Fig. 2*C* and *E*). Dye-loading of individual neurons via whole-cell patch-clamp enabled Na^+ imaging in apical dendrites (Fig. 2*D*). These underwent regular Na^+ oscillations as well, which at a distance of 50–100 μm from the cell body exhibited a similar mean amplitude to that in the somata ($P = 0.329$), amounting to 10.3 ± 4.7 mM (range: 4.1–28.9 mM; median: 8.9 mM; $n = 100$ dendritic segments, $N = 5$) (Fig. 2*D* and *E*).

In acute tissue slices derived from transgenic mice, expressing ATeam in neurons ($N = 7$) (Trevisiol *et al.* 2017), perfusion with $0Mg^{2+}$/BIC resulted in a slow decline in the ΔATeam ratio in both somata and primary apical dendrites of CA1 pyramidal neurons, which partly recovered upon reperfusion with standard ACSF (Fig. 2*F*). After 30 min of $0Mg^{2+}$/BIC, [ATP] in cell bodies had decreased by 0.30 ± 0.16 mM (range: 0.04–0.58 mM, median: 0.29 mM; $n = 103$) (Fig. 2*G*). In dendrites, [ATP] decreased by 0.39 ± 0.16 mM (range: 0.13–0.64 mM, median: 0.42 mM; $n = 36$ dendrites), which is a significantly larger decline as compared to somata ($P = 0.007$) (Fig. 2*G*). Notably the ΔATeam ratio does not change under control conditions within this time frame (Lerchundi *et al.* 2019*a*), indicating that the slow decline observed in the present study was indeed related to the ongoing activity induced by the dis-inhibition.

In summary, these experiments demonstrate that recurrent network activity and global network Na^+ oscillations in somata and dendrites of CA1 pyramidal neurons are accompanied by a slow and steady decrease in [ATP] in these compartments that amounts to 0.3–0.4 mM after 30 min.

Changes in $[Na^+]_i$ and $[ATP]_i$ evoked by afferent fibre stimulation

With recurrent network activity and ongoing global Na^+ oscillations, a slow decrease in neuronal [ATP] over time was observed. Next, we analysed if distinct transient increases in $[Na^+]_i$ are accompanied by detectable changes in $[ATP]_i$. Earlier work has shown stimulation of glutamatergic afferents results in transient increases in $[Na^+]_i$ in cell bodies and dendrites of CA1 pyramidal neurons mainly due to Na^+ influx through ionotropic glutamate receptor channels (Rose & Konnerth, 2001; Langer & Rose, 2009; Miyazaki & Ross, 2017). To induce transient Na^+ influx into neurons, we thus performed a burst stimulation of afferent Schaffer collaterals (10 stimuli at 50 Hz) at a distance of approximately 100–150 μm to the analysed cells or ROIs in acute hippocampal slices.

In neuronal somata of acutely isolated tissue slices, bolus-loaded with SBFI-AM, electrical stimulation of Schaffer collaterals induced a transient increase in $[Na^+]_i$ which reached its maximal amplitude of 24.0 ± 17.7 mM (range: 5.6–88.9 mM, median: 18.8 mM; $n = 53$, $N = 7$) after 7.8 ± 3.3 s (range: 1.9–14.6 s, median: 7.1 s) (Fig. 3*A*, *C* and *G*). $[Na^+]_i$ transients evoked in apical dendrites of cells loaded by whole-cell patch-clamp were significantly

larger, amounting to 33.9 ± 21.3 mM (range: 7.7–96.9 mM, median: 28.2 mM; $n = 82$ dendritic segments, $N = 21$; $P = 0.006$) (Fig. 3*B* and *C*). At the same time, their peak was reached significantly faster than in cell bodies (1.0 ± 0.9 s, range: 0.1–5.7 s, median: 0.7 s; $P < 0.001$) (Fig. 3*G*). Recovery from Na^+ transients was accomplished within 1–1.5 min in somata and within about 20–30 s in dendrites (Fig. 3*A* and *B*). Both the inward currents

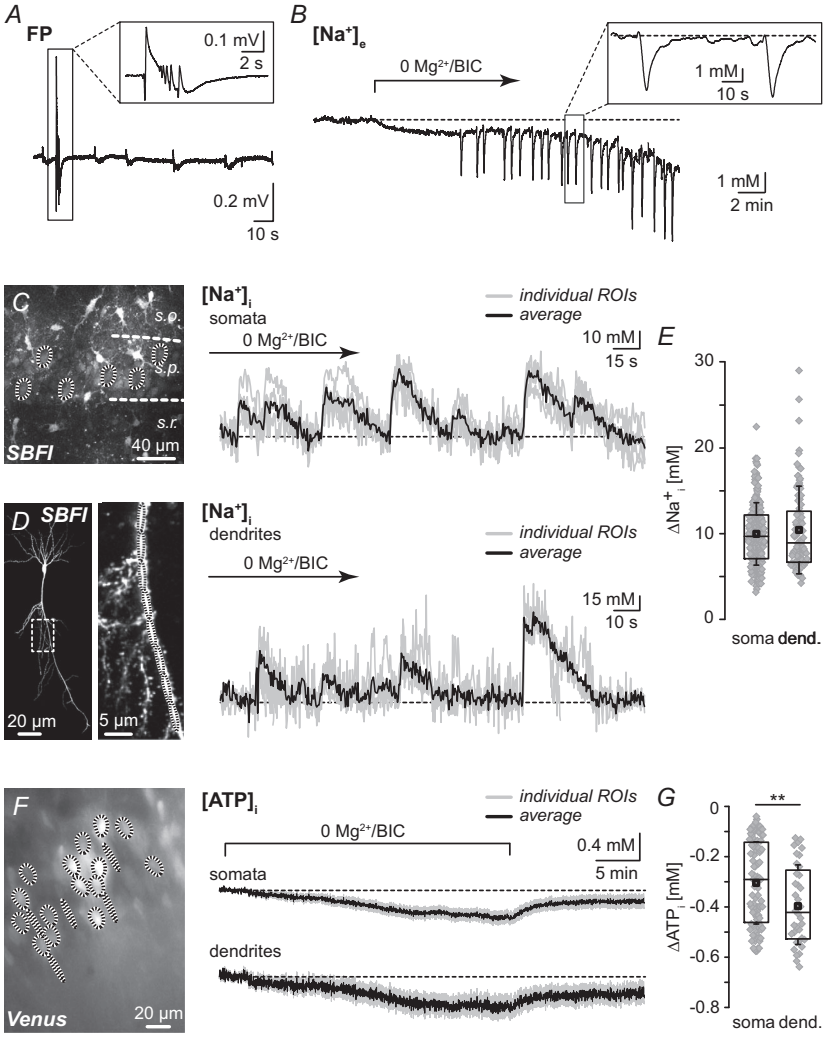

Figure 2. Network [Na^+] oscillations and resulting changes in [ATP]$_i$
A, field-potential recording from the CA1 stratum pyramidale in an acute tissue slice during perfusion with Mg^{2+}-free saline containing 10 µM bicuculline methiodide ($0Mg^{2+}$/BIC). Note the occurrence of short biphasic changes as well as larger epileptiform bursts. The box shows an epileptiform burst in more detail. *B*, changes in $[Na^+]_e$ evoked by perfusion with $0Mg^{2+}$/BIC. The box shows an enlargement of two $[Na^+]_e$ transients. *C*, left, two-photon image of the CA1 pyramidal cell layer (s.p.) of an acute hippocampal slice loaded with SBFI-AM. Dotted lines indicate ROIs representing cell bodies of pyramidal neurons from which fluorescence was analysed shown in *E*. s.o., stratum oriens; s.r., stratum radiatum. Note the presence of brightly labelled presumed astrocytes in the field of view. Right, $[Na^+]_i$ signals in somata observed during perfusion with $0Mg^{2+}$/BIC. *D*, left, maximal intensity projection image of a neuron in an acute slice, filled with SBFI through a patch pipette that was later withdrawn. The box indicates the area shown on the right at larger scale, where the dotted lines indicate ROIs from which fluorescence was analysed as shown on the right. Right, $[Na^+]_i$ signals in dendritic regions of interest during perfusion with $0Mg^{2+}$/BIC. *E*, box-and-whisker plot showing peak changes of $[Na^+]_i$ transients in the presence of $0Mg^{2+}$/BIC in somata and dendrites. *F*, left, Venus fluorescence of CA1 pyramidal neurons expressing ATeam in an acute tissue slice. Dotted lines indicate ROIs from which fluorescence was analysed shown on the right. Right, changes in [ATP] during perfusion with $0Mg^{2+}$/BIC as indicated. *G*, box-and-whisker plot showing peak changes in [ATP] following a 30 min perfusion with $0Mg^{2+}$/BIC. *C*, *D* and *F*: shown are traces from individual ROIs (grey) as well as the average thereof (black trace). *E* and *G* depict means (squares), IQR (box), median (line), SD (whiskers) and all single data points (grey diamonds).

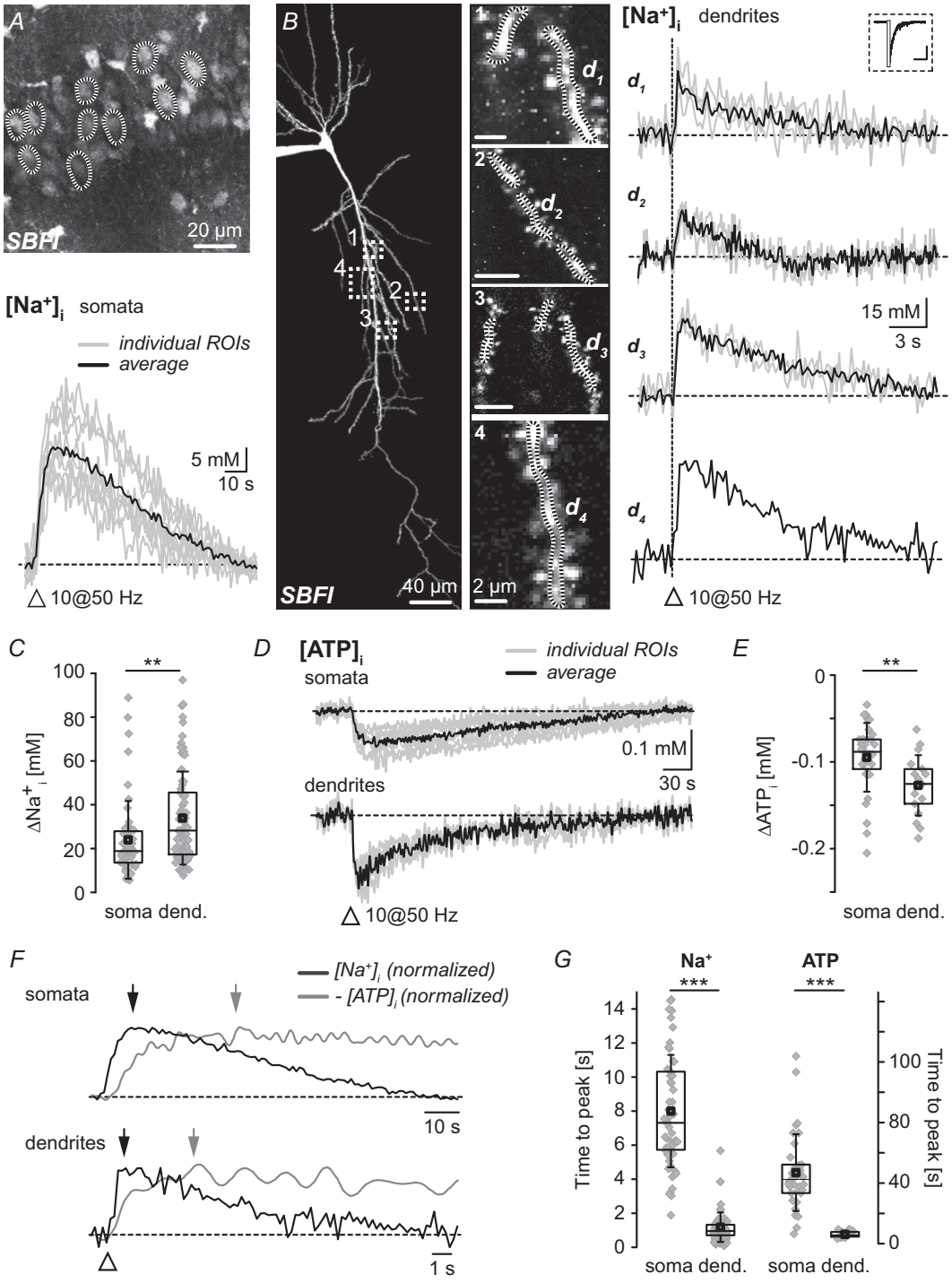

Figure 3. Changes in $[Na^+]_i$ and $[ATP]_i$ induced by afferent stimulation
A, top, two-photon image of the pyramidal cell layer of an acute hippocampal slice loaded with SBFI-AM. Dotted lines indicate ROIs representing cell bodies of pyramidal neurons from which fluorescence was analysed as shown below. Note the presence of brightly labelled presumed astrocytes in the field of view. Bottom, somatic $[Na^+]_i$ signals induced by synaptic stimulation (triangle). *B*, left, maximal intensity projection image of a CA1 pyramidal neuron filled with SBFI through a patch pipette. The boxes (1–4) delineate areas enlarged on the right, where dendritic ROIs from which measurements were taken are indicated by lines. Right, dendritic $[Na^+]_i$ signals in response to synaptic stimulation (triangle). The respective somatic inward current is depicted in the box on the upper right (stimulation artifact blanked, scale: 0.5 nA/1 s). *C*, box-and-whisker plot showing peak amplitudes of $[Na^+]_i$ transients in somata and dendrites. *D*, changes in [ATP] in somata and dendrites in an acute tissue slice evoked by afferent stimulation (triangle). *E*, box-and-whisker plot showing synaptically induced peak changes

resulting from the stimulation (see inset in Fig. 3*B*) as well as the dendritic Na^+ transients were blocked by tetrodotoxin (TTX; 0.5 μM), demonstrating that their dependency on the opening of voltage-gated Na^+ channels and the generation of action potentials, respectively ($n = 4$, $N = 4$; data not shown).

Imaging of the ΔATeam ratio in acute tissue slices showed that afferent stimulation was also accompanied by a transient decrease in the [ATP] of somata and dendrites (Fig. 3*D*). The peak amplitude in dendrites was larger as compared to somata (somata: 0.09 ± 0.04 mM, range: 0.03–0.21 mM, median: 0.09 mM; $n = 32$, $N = 4$; and dendrites: 0.13 ± 0.03 mM, range: 0.06–0.19 mM, median: 0.13; $n = 17$ dendrites, $N = 4$; $P = 0.007$) (Fig. 3*E*). Moreover, [ATP] dropped much faster in dendrites as compared to cell bodies (time to peak in dendrites: 6.2 ± 2.1 s, range: 3.3–9.5 s, median: 5.6 s; and in cell bodies: 47.0 ± 25.4 s, range: 6.5–123.9 s, median: 42.5 s; $P < 0.001$) (Fig. 3*G*). Full recovery to baseline took approximately 5–6 min in both compartments (Fig. 3*D*).

An overlay and peak normalization of evoked $[Na^+]_i$ transients and changes in $[ATP]_i$ visualizes the time courses of both signals (Fig. 3*F*). It illustrates that changes in [ATP] basically start in parallel to those in $[Na^+]$ in a given compartment. Their peaks, however, are considerably delayed and reached only after $[Na^+]_i$ has already partially recovered to baseline. Recovery of $[ATP]_i$ is essentially not seen before $[Na^+]_i$ has fully recovered, and thus lags many minutes behind.

Overall, these results show that a single burst stimulation of afferent fibres results in a transient increase in $[Na^+]$ in CA1 pyramidal neurons, which exhibits a significantly larger amplitude and faster kinetics in dendrites as compared to cell bodies. Moreover, the stimulation evokes a transient decrease in [ATP] in dendrites and somata. Amplitude and time course of the drop in $[ATP]_i$ essentially mirror those in $[Na^+]$ in the respective compartment, albeit with much slower kinetics.

Changes in $[Na^+]_i$ and $[ATP]_i$ induced by application of glutamate

The results presented so far demonstrated that somatic and dendritic $[Na^+]_i$ transients resulting from synchronized excitatory input into CA1 pyramidal neurons are accompanied by delayed decreases in $[ATP]_i$ in both compartments. We next tested the effect of a direct application of glutamate on intracellular $[ATP]_i$. These experiments were performed in the presence of TTX (0.5 μM) to prevent the generation of action potentials.

In the first set of experiments, acute tissue slices were exposed to a bath perfusion with 1 mM glutamate for 10 s. As expected, this elicited a strong and long-lasting transient increase in $[Na^+]_i$ in neuronal somata ($n = 45$, $N = 6$) to 53.3 ± 27.1 mM (range: 9.8–100.9 mM, median: 44.2 mM; $n = 39$, $N = 6$). Its peak was reached after 30.7 ± 7.5 s (range: 18.9–53.8 s, median: 29.6 s), full recovery to baseline took on average 220 s (Fig. 4*A*, *B* and *F*). In dendrites ($n = 30$ dendritic segments, $N = 5$), average $[Na^+]_i$ elevations amounted to 39.5 ± 32.1 mM (range: 9.1–134.6 mM, median: 27.7 mM; $P = 0.056$) (Fig. 4*A* and *B*). While this was not significantly different from somatic peak amplitudes, the rise time of dendritic $[Na^+]_i$ increases was significantly faster ($P < 0.001$) than in somata (9.7 ± 4.0 s, range: 3.8–17.6 s, median: 8.9 s) (Fig. 4*F*). On average, dendritic $[Na^+]_i$ increases recovered back to baseline within about 85 s (Fig. 4*A* and *E*).

Bath application of glutamate also resulted in a relatively slow and strong decrease in cellular $[ATP]_i$ (Fig. 4*C*). In somata ($n = 139$, $N = 6$), [ATP] decreased by 0.46 ± 0.18 mM (range: 0.14–1.10 mM, median: 0.42 mM) within 109.8 ± 21.5 s (range: 72.4–168.9 s, median: 105.4 s). (Fig. 4*D* and *F*). Dendritic [ATP] dropped significantly faster (time to peak: 85.9 ± 24.9 s, range: 56.2–144.8 s, median: 76.7 s; $P < 0.001$) and to lower levels (decrease by 0.56 ± 0.20 mM, range: 0.23–1.25 mM, median: 0.51 mM; $P = 0.014$; $n = 30$ dendritic segments, $N = 5$) (Fig. 4*D* and *F*). About half of the somata and dendrites recorded fully recovered to initial baseline levels, while the other half recovered to a stable level that was ∼0.1 mM below the initial baseline; both processes required about 8–12 min (Fig. 4*E*).

Again, an overlay of peak-normalized averaged traces revealed that changes in $[ATP]_i$ induced with bath application of glutamate began with those in $[Na^+]_i$ in each compartment, but exhibited a significantly delayed peak and displayed much slower kinetics. To better visualize the apparent coincidence of the first phase of both signals, we calculated the first derivative of the normalized changes in $[ATP]_i$. The resulting trace (green trace in Fig. 4*E*) clearly delineates that the decline in $[ATP]_i$ was indeed coincident with the rise in $[Na^+]_i$ and slowed down with the recovery of $[Na^+]_i$ to baseline, indicative of a declining consumption of ATP in both compartments.

In a second set of experiments, glutamate (1 mM) was applied focally through a fine glass pipette positioned

[ATP] in somata and dendrites. *F*, overlay of the averaged somatic $[Na^+]_i$ signal (black) and the averaged change in somatic [ATP] (grey, inverted) upon synaptic stimulation, normalized to their peaks (arrows). Bottom, same illustration for dendrites. *G*, box-and-whisker plot showing the time to peak of the synaptically induced $[Na^+]_i$ and $[ATP]_i$ transients. *A*, *B* and *D*: shown are traces from individual ROIs (grey) as well as the average thereof (black trace). *C*, *E* and G depict means (squares), IQR (box), median (line), SD (whiskers) and all single data points (grey diamonds).

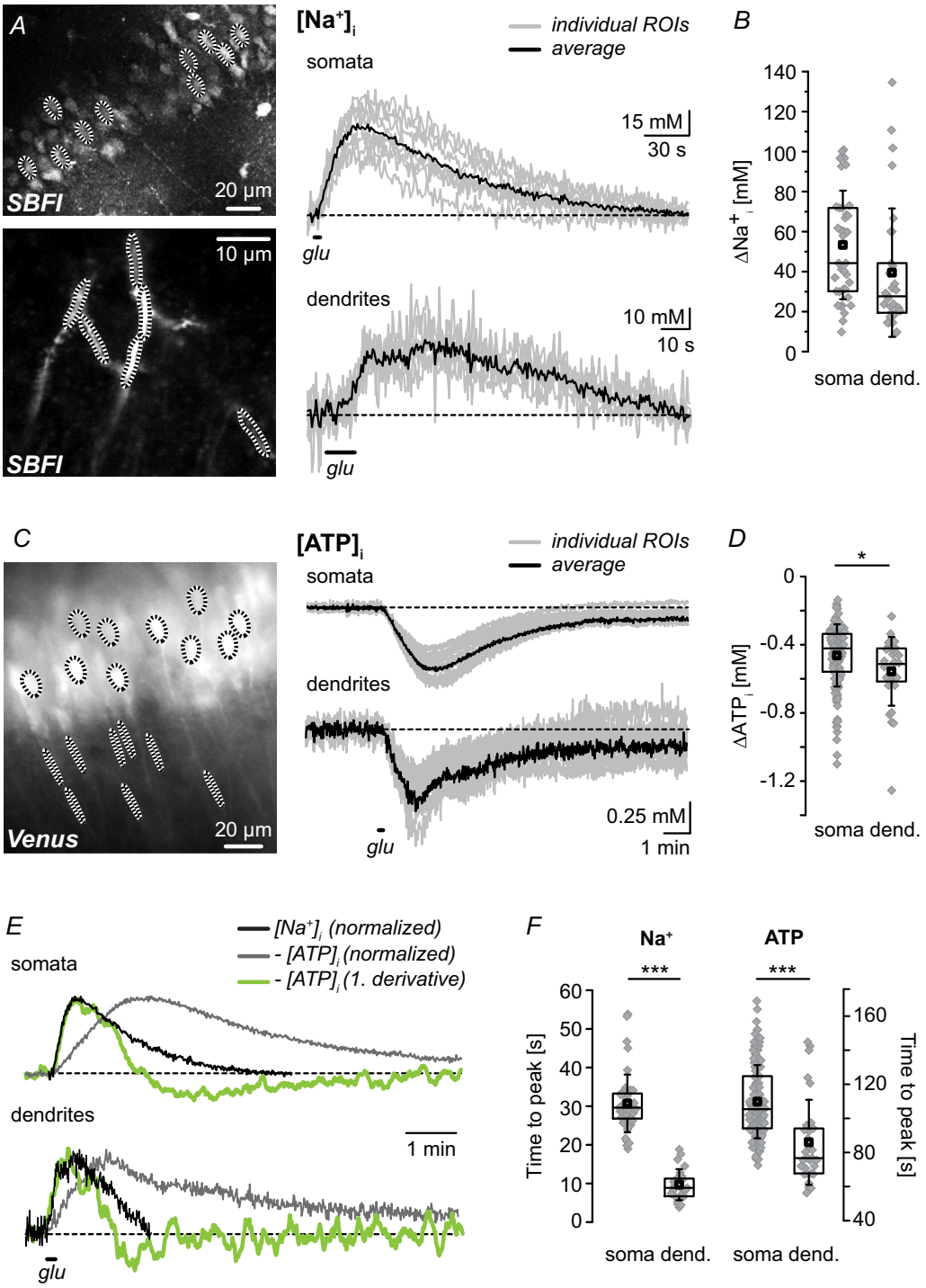

Figure 4. Changes in $[Na^+]_i$ and $[ATP]_i$ induced by bath application of glutamate
A, left, two-photon image of an acute hippocampal slice loaded with SBFI-AM (top). Bottom left shows a dendrite loaded with SBFI during whole-cell patch-clamp. Dotted lines indicate ROIs from which fluorescence was analysed as shown on the right. Right, $[Na^+]_i$ signals induced by bath perfusion of glutamate (1 mM/10 s) in somata and dendrites. *B*, box-and-whisker plot showing glutamate-induced peak changes of $[Na^+]_i$ in somata and dendrites. *C*, left, wide-field image of neuronal ATeam fluorescence (acute brain slice). Dotted lines indicate ROIs from which fluorescence was analysed as shown on the right. Right, changes in the [ATP] in somata (top) and dendrites (bottom) upon bath perfusion of glutamate (1 mM/10 s). *D*, box-and-whisker plot showing glutamate-induced peak changes in [ATP] in somata and dendrites. *E*, top, overlay of the averaged somatic $[Na^+]_i$ signal (black) and the averaged change in somatic [ATP] (grey, inverted) upon glutamate application, normalized to their peak. Moreover, the first derivative of the normalized change in somatic [ATP] (green, inverted) is shown. Bottom, same

close (∼10 μm) to apical dendrites of CA1 neurons in organotypic slices to evoke local Na^+ influx (Fig. 5*A*). ROIs, encompassing dendritic sections of ∼10 μm in length were set to study resulting $[Na^+]_i$ transients along dendrites (Fig. 5*A*). Pressure application for 50 ms ($n = 14$, $N = 6$) resulted in a $[Na^+]_i$ increase of 12.0 ± 4.6 mM (range: 5.0–18.16 mM, median: 12.6 mM) in ROIs in the immediate vicinity (∼10 μm) of the application pipette, while in sections further away, changes in $[Na^+]_i$ could hardly be resolved (Fig. 5*A*). Increasing the duration of the pressure application ($n = 9$–15, $N = 5$) resulted in increased peak amplitudes of $[Na^+]_i$ elevations (100 ms: 30.2 ± 11.2 mM, range: 18.2–48.0 mM, median: 30.1 mM; 200 ms: 33.2 ± 29.9 mM, range: 12.9–106.2 mM, median: 22.1 mM; 500 ms: 61.7 ± 24.8 mM, range: 25.6–117.7 mM, median: 62.3 mM) (Fig. 5*B*). At the same time, their spatial restriction was lost and at 500 ms application, all dendritic sections in the field of view showed $[Na^+]_i$ transients (Fig. 5*A*).

The same stimulation paradigm and protocol were then employed while imaging [ATP] with ATeam in dendrites ($n = 31$ cells, $N = 3$). To determine the detection threshold, all data points obtained from a given ROI during a 1–2 min period of baseline were averaged to obtain a mean value and their standard deviation was calculated. The latter was multiplied by two and subtracted from the mean, defining the minimum threshold for signal detection as shown in Fig. 5*C* ('2SD'). With a typical detection threshold of 0.02–0.03 mM in this set of experiments, pressure application of glutamate to dendrites for 50 ms did not result in a detectable change in [ATP] in the vast majority (29/31) of dendritic segments recorded from (Fig. 5*C* and *D*). Upon application for 100 ms, a decrease in [ATP] by 0.03–0.06 mM could be resolved in 7 out of 31 dendritic sections (overall average peak decrease: 0.01 ± 0.019 mM; range: 0–0.057 mM; median: 0 mM); 19 out of 31 dendrites responded to application for 200 ms (overall mean: 0.030 ± 0.026 mM, range: 0–0.074 mM, median: 0.034 mM). All dendritic sections (31/31) showed a decrease in [ATP] to pressure application of glutamate for 500 ms, averaging 0.071 ± 0.022 mM (range: 0.040–0.120 mM, median: 0.068 mM).

In summary, these results show that large, global $[Na^+]_i$ transients, evoked by bath application of glutamate in both dendrites and somata, result in a delayed decline in [ATP] in both compartments. In contrast to this, glutamate-induced local $[Na^+]_i$ transients that are restricted to small sections of dendrites are not accompanied by detectable changes in dendritic [ATP].

Discussion

In the present study, we analysed the relation between activity-induced Na^+ transients and intracellular ATP levels in CA1 pyramidal neurons of the mouse hippocampus using the Na^+-sensitive indicator dye SBFI and the nanosensor ATeam. Calibration of ATeam in neurons revealed an apparent K_D of the sensor of 2.6 mM. Disinhibition of slices, burst stimulation of glutamatergic afferent fibres, or bath application of glutamate induced global $[Na^+]_i$ signals that comprised dendrites as well as somata of CA1 neurons. Global $[Na^+]_i$ transients were accompanied by transient decreases in [ATP] in both compartments. The relative peak amplitude and kinetics of these $[ATP]_i$ changes largely correlated with the properties of the changes in $[Na^+]_i$ in the given compartment. In contrast to global $[Na^+]_i$ transients, induction of a locally restricted Na^+ influx into dendrites by focal application of glutamate did not result in a detectable change in dendritic [ATP].

Properties of activity-related neuronal Na^+ elevations

Influx of Na^+ is a major mechanism for the generation of plasma membrane depolarization. Depending on the pattern of activity, this can be accompanied by transient changes in the extracellular $[Na^+]$. Earlier work performed in the cat cortex *in vivo* as well as in rat hippocampal tissue slices has shown that electrical stimulation at 15–20 Hz for 10 s results in a drop in the extracellular $[Na^+]$ by 5–10 mM (Dietzel *et al.* 1982; Zanotto & Heinemann, 1983). In the present study, burst-like neuronal activity induced by $0Mg^{2+}$/BIC saline was accompanied by transient decreases in extracellular $[Na^+]$ by 1–4 mM. These bursts only lasted ∼5 s, and the magnitude of $[Na^+]$ decreases in relation to activity pattern is thus rather comparable between the different studies.

$[Na^+]_i$ transients are, for example, generated upon opening of voltage-gated Na^+ channels in axons (Fleidervish *et al.* 2010; Baranauskas *et al.* 2013; Ona-Jodar *et al.* 2017). Similarly, bursts of back-propagating action potentials cause transient $[Na^+]$ elevations in dendrites and spines, albeit of much lower peak amplitude (Jaffe *et al.* 1992; Rose *et al.* 1999; Ona-Jodar *et al.* 2017). A main route for Na^+ influx is postsynaptic ionotropic glutamate receptors activated by synaptic release or exogenous application of glutamate (Lasser-Ross & Ross, 1992; Knopfel *et al.* 2000; Rose & Konnerth, 2001; Meier *et al.* 2006; Bennay *et al.* 2008; Miyazaki & Ross, 2017).

illustration for dendrites. *F*, box-and-whisker plot showing the time to peak of the glutamate-induced $[Na^+]_i$ and $[ATP]_i$ transients. *A* and *C*: shown are traces from individual ROIs (grey) as well as the average thereof (black traces). *B*, *D* and *F* depict means (squares), IQR (box), median (line), SD (whiskers) and all single data points (grey diamonds). [Colour figure can be viewed at wileyonlinelibrary.com]

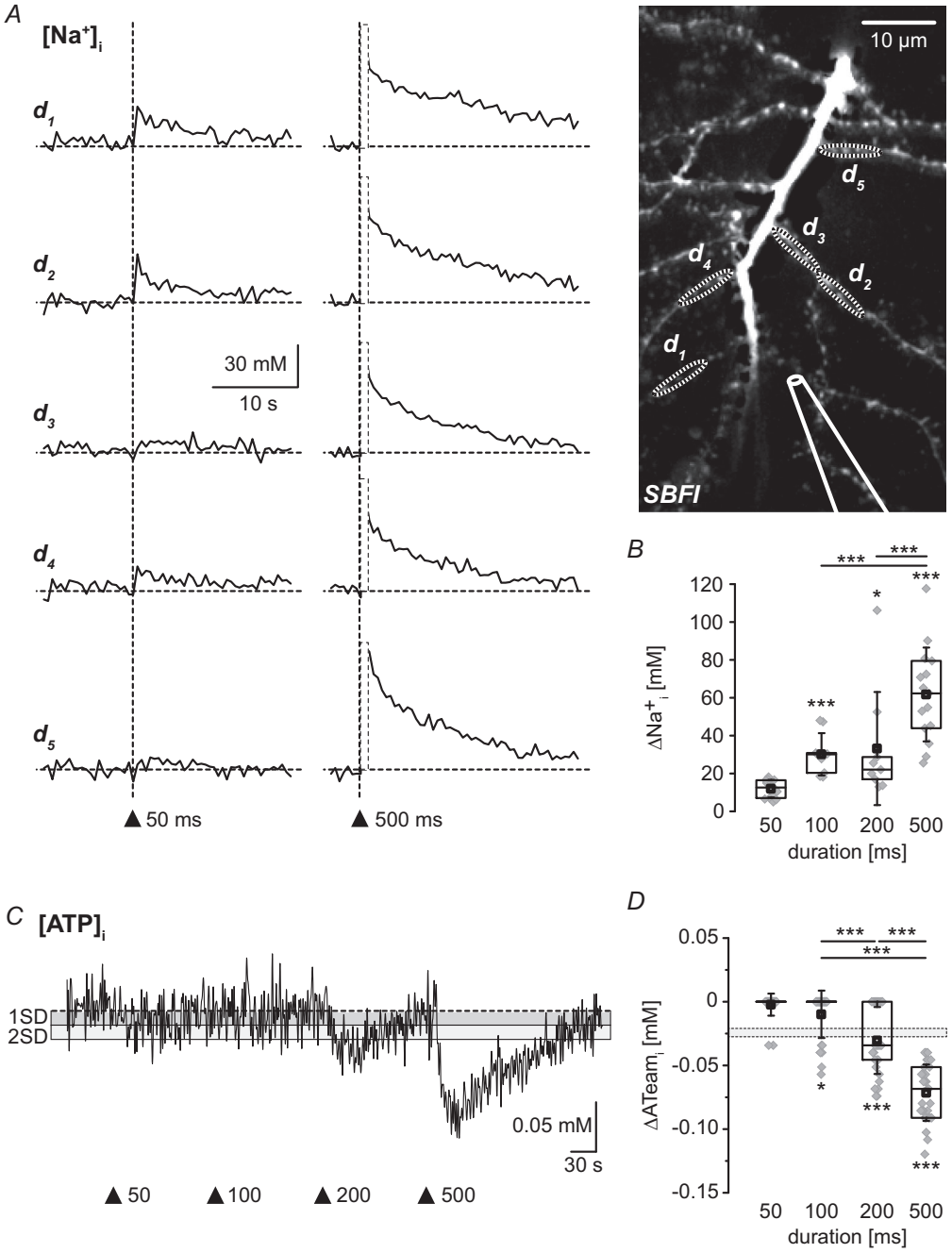

Figure 5. Changes in $[Na^+]_i$ and $[ATP]_i$ induced by local puff application of glutamate
A, left, $[Na^+]_i$ signals induced by puff application of glutamate (1 mM) for 50 ms and 500 ms (arrowheads) in dendritic section d_1–d_5 as shown on the right. Note that application artifact induced by a pressure application for 500 ms was blanked in this recording. Right, two-photon image of part of the dendritic tree of a neuron in an organotypic slice loaded with SBFI during whole-cell patch-clamp. Dotted lines indicate ROIs d_1–d_5 from which fluorescence was analysed as shown on the left. *B*, box-and-whisker plot showing glutamate-induced peak changes of $[Na^+]_i$ in dendrites for different puff durations. *C*, changes in the dendritic [ATP] in an organotypic slice upon puff application of glutamate for 50, 100, 200 and 500 ms as indicated (averaged trace from all ROIs obtained from one experiment). *D*, box-and-whisker plot showing glutamate-induced peak changes in dendritic [ATP] for glutamate applications as indicated. The dotted box delineates the average detection threshold in this set of experiments. *B* and *D* depict means (squares), IQR (box), median (line), SD (whiskers) and all single data points (grey diamonds).

Ionotropic glutamate receptors also represent the most important influx pathways underlying synchronous oscillations of somatic $[Na^+]_i$ during recurrent neuronal network activity in hippocampal tissue slices as shown here and described in detail previously (Karus *et al.* 2015). In the present study, we moreover demonstrate that $[Na^+]_i$ oscillations also comprise the apical dendritic tree of CA1 neurons, indicating that they occur in the entire cell. In addition, global cellular $[Na^+]_i$ transients, ranging from 20–40 mM, were induced by burst stimulation of the Schaffer collateral pathway and by a 10 s bath application of glutamate.

As opposed to such global events, $[Na^+]_i$ transients can also be local and occur in parts of a dendrite and adjacent spines only, e.g. upon more locally restricted stimulation of excitatory fibres and/or postsynaptic sites (Lasser-Ross & Ross, 1992; Knopfel *et al.* 2000; Rose & Konnerth, 2001; Meier *et al.* 2006; Bennay *et al.* 2008; Mondragao *et al.* 2016; Miyazaki & Ross, 2017). In the present study, brief (50–100 ms) pressure application of glutamate close to a dendrite induced $[Na^+]_i$ increases that were largely confined to dendritic sections within a distance of 10–15 µm from the tip of the application pipette.

The spatial extent of activity-related $[Na^+]_i$ elevations as reported by chemical Na^+ indicators can thus vary strongly, depending on their underlying mechanism and on the pattern of activity. High-affinity Ca^{2+}-sensitive dyes like Oregon Green or Fura-2 exert a considerable buffering of Ca^{2+}, thereby causing a distortion of Ca^{2+} signals influencing both their amplitude and their spatial occurrence (Maravall *et al.* 2000). This, however, is not the case for Na^+ transients determined using SBFI. The K_D of SBFI is well above the baseline $[Na^+]_i$ (present study: 42 mM and Rose *et al.* 1999; Sheldon *et al.* 2004; Meier *et al.* 2006). Even for whole-cell patch-clamp measurements, where SBFI is routinely used at concentrations of around 1 mM, it does not visibly buffer Na^+ inside cells (Mondragao *et al.* 2016).

Upon its influx, Na^+ has to be extruded from neurons to maintain low baseline $[Na^+]_i$ and thereby maintain driving forces for Na^+-based electrical signalling. Na^+ export is achieved by the NKA, which is activated by rises in $[Na^+]_i$ (Thompson & Prince, 1986; Sweadner, 1995; Therien & Blostein, 2000; Larsen *et al.* 2016). Recovery from global $[Na^+]_i$ signals is, therefore, strictly dependent on NKA and on an intact energy metabolism (Lees, 1991; Erecinska & Silver, 1994; Somjen, 2002; Mondragao *et al.* 2016). For recovery from local $[Na^+]_i$ transients, an additional mechanism was demonstrated to come into play, namely the intracellular diffusion of Na^+ to non-stimulated areas, a phenomenon described from axon initial segments (Fleidervish *et al.* 2010) as well as dendrites and dendritic spines (Rose & Konnerth, 2001; Mondragao *et al.* 2016; Miyazaki & Ross, 2017). In primary apical dendrites largely devoid of spines, it was estimated that Na^+ diffused with a diffusion coefficient of approximately 330 $\mu m^2\ s^{-1}$ (Mondragao *et al.* 2016). This is much faster as compared to (buffered) diffusion of calcium (~13 $\mu m^2\ s^{-1}$) (Yuste *et al.* 2000), and enables a rapid lateral redistribution Na^+ from the site of influx solely driven by its concentration gradient (Mondragao *et al.* 2016).

Different activity patterns neuronal ATP levels

In the present study, we employed the FRET-sensor ATeam for detection of intracellular ATP. Since the description of ATeam and its variants in 2009 (Imamura *et al.* 2009), ATP sensors have been constantly adapted and/or newly designed (Nakano *et al.* 2011; Yaginuma *et al.* 2014; Arai *et al.* 2018; Mendelsohn *et al.* 2018; Lobas *et al.* 2019), also for detection of ATP in organelles (Imamura *et al.* 2009; Rueda *et al.* 2015; Suzuki *et al.* 2018). Moreover, a ratiometric sensor for imaging of the ATP-to-ADP ratio (PercevalHR) is available (Tantama *et al.* 2013).

ATeam exhibits a relatively low K_D in *in vitro* calibrations (around 0.25 mM at room temperature and 1.2 mM at 37°C), suggesting that it might be saturated inside cells (Imamura *et al.* 2009). Our recent work performed in hippocampal tissue slices provided evidence that this is not the case by demonstrating that ATeam reports an increase in astrocytic ATP levels in response to an increase in the extracellular potassium concentration (Lerchundi *et al.* 2019*b*). The *in situ* calibration of ATeam presented here supports this notion, revealing an apparent K_D for ATP of 2.6 mM under our experimental conditions. Such a change in properties does not seem to be exclusive to ATeam, since an apparent decrease in binding affinity inside cells was, for example, also reported from the ratiometric fluorescent ATP indicator Queen (Yaginuma *et al.* 2014). Neither the relative increase in ATP levels induced by high K^+ nor their decrease upon blocking cellular metabolism reported by ATeam was altered when elevating the temperature by 10°C (Lerchundi *et al.* 2019*b*). The latter observation indicates that its K_D is not strongly temperature-dependent inside cells, which is also different from the results obtained *in vitro* (Imamura *et al.* 2009).

Together with the reported [ATP] of ~2 mM in neurons (Fukuda *et al.* 1983; Chinopoulos *et al.* 2000; Ainscow *et al.* 2002; Mollajew *et al.* 2013; Rangaraju *et al.* 2014; Pathak *et al.* 2015), these results strongly suggest that ATeam is well suited to monitor changes in $[ATP]_i$. As a rule of thumb, the apparent K_D of 2.6 mM indicates that ATeam will be able to detect *changes* in the ATP concentration at baseline ATP levels between 0.26 and a theoretical maximum of 26 mM (but see Fig. 1 it is practically close to saturation at ~10 mM). At the presumed baseline ATP concentration of 2 mM, the sensor works close to its K_D and is thus in its optimal 'working range', responding to changes in

ATP with relatively large changes in fluorescence (see Fig. 1). There are also other ATeam variants available that enable detection of very small changes in ATP (e.g. ATeam3.10; Imamura *et al.* 2009). However, under physiological conditions, lower K_D sensors are already completely saturated inside cells and thereby not applicable in this kind of experiment and preparation.

All stimulation paradigms employed in the present study, except brief local pressure application of glutamate onto dendrites, resulted in well-detectable decreases in somatic and dendritic [ATP]. With a detection threshold of 0.02–0.03 mM, changes in $[ATP]_i$ were roughly in the range of 0.1–0.6 mM. For a given stimulation there was a large variance in the peak amplitude of $[ATP]_i$ decreases between individual cells and also between dendritic regions of a given cell. This remarkable variability may reflect a different density and intracellular distribution of mitochondria (and capacity for rapid ATP production): cells or dendrites that experienced a relatively large decrease in $[ATP]_i$ in response to a given stimulation might have hosted fewer mitochondria than those showing a small decrease. Mitochondria in neurons and astrocytes generally exist in two pools, one of them stationary and the other one in motion (Misgeld & Schwarz, 2017). The latter pool apparently serves to enable a directed movement and arrest of mitochondria to sites of increased energy demand (Jackson & Robinson, 2018). Based on these findings, one could speculate that a repeated stimulation with glutamate will increase the number of mitochondria close to Na^+ (and Ca^{2+}) influx sites, thereby increasing the local capacity for rapid ATP production. Subsequent challenges with glutamate might then result in smaller decreases in $[ATP]_i$.

In dendrites, ATP levels generally dropped to lower levels as compared to cell bodies. Moreover, dendritic [ATP] decreased significantly faster than somatic [ATP] in response to afferent stimulation and bath application of glutamate. This suggests that the ATP availability in dendrites is more restricted and/or that dendritic ATP consumption is more pronounced than that of somata. In both compartments, $[ATP]_i$ decreases were fully reversible upon fibre stimulation or local pressure application of glutamate for 200–500 ms. This was in contrast to recurrent network activity or bath application of glutamate after which ATP levels did not always fully return to initial baseline, but remained at a slightly decreased level (around −0.1 mM) for the duration of the recording. A similar phenomenon was reported from astrocytes in culture upon bath application of glutamate (Winkler *et al.* 2017), suggesting that with strong stimulation (and Na^+ influx, respectively), cells establish a new steady-state.

Upon disinhibition of slices and neuronal network activity accompanied by $[Na^+]_i$ oscillations, we observed a slowly developing decline in neuronal [ATP] by 0.3–0.4 mM. This is somewhat lower as reported before based on estimates of [ATP] using the sensor ATeam1.03 (Toloe *et al.* 2014). A reduction in this range might alter the conductance of K_{ATP} channels, resulting in a dampening of neuronal excitability, thereby executing an anti-convulsant effect (Proks & Ashcroft, 2009; Mollajew *et al.* 2013; Toloe *et al.* 2014; Martinez-Francois *et al.* 2018).

Bath application of glutamate for 10 s had the strongest impact on neuronal [ATP], resulting in a drop by 0.5–0.6 mM. At an assumed neuronal [ATP] of 2 mM, even such a relatively large decrease in ATP levels would probably not directly restrict the activity of the NKA. The NKA has both a high-affinity binding site (K_D 0.1–0.2 μM) and a regulatory binding site for ATP (K_D 0.2–0.4 mM) (Lees, 1991; Blanco & Mercer, 1998; Kaplan, 2002) and earlier studies have estimated that its activity declines only when ATP levels fall below 0.4 mM (Dagani & Erecinska, 1987). This is also evident from the efficient recovery from the large $[Na^+]_i$ increases that were seen under these conditions. Notably, and as mentioned above, the changes in $[ATP]_i$ as detected during the different stimulation paradigms might, however, exert an effect on neuronal membrane potentials by increasing the opening of K_{ATP} channels.

Local pressure application of glutamate for 50 ms close to a dendrite, as opposed to all other stimulation paradigms, generally did not result in a detectable change in $[ATP]_i$, while at the same time inducing a transient $[Na^+]_i$ increase by about 12 mM. Increasing the duration of the pressure application increased the ratio of responding dendrites, until at 500 ms, all dendritic sections tested showed a decrease in [ATP]. This suggests that localized activation of glutamate receptors changes dendritic $[ATP]_i$ by less than 0.02–0.03 mM, which is not expected to exert a significant effect on the activity of the NKA or of K_{ATP} channels.

Relation between sodium and ATP

Previous work has demonstrated a link between Na^+ influx and ATP levels in different cell types including neurons (e.g. Chinopoulos *et al.* 2000; Mollajew *et al.* 2013). Here, such a correlation was found for patterns of activity which induced global $[Na^+]_i$ transients that comprised both neuronal somata and dendrites. For a given stimulation paradigm, the amplitude of $[Na^+]_i$ transients and the change in $[ATP]_i$ were positively correlated. Moreover, we found that the kinetics of changes in $[ATP]_i$ generally followed those in $[Na^+]_i$. However, while $[ATP]_i$ essentially began to drop as soon as changes $[Na^+]_i$ began to rise (see Fig. 4*E*), the peak of $[ATP]_i$ changes was delayed as compared to the peak of $[Na^+]_i$ transients and recovery to baseline [ATP] took significantly longer. These results indicate that $[Na^+]_i$ loads and activation of the NKA are indeed major

determinants of neuronal ATP consumption. Activation of glutamatergic signalling as performed in the present study, however, not only causes a rise in $[Na^+]_i$, but will, for example, also evoke an elevation of intracellular calcium. This will most likely result in the activation of other ATP-consuming processes, including the plasma membrane Ca^{2+}-ATPase and/or the SERCA (Clapham, 2007), contributing to the observed drop in $[ATP]_i$. At presynaptic terminals, ATP will additionally be required by the vacuolar-type H^+-ATPase to regenerate the H^+ gradient required for neurotransmitter accumulation in presynaptic vesicles (Cotter *et al.* 2015; Sobieski *et al.* 2017).

The time course and temporal relation of changes in $[Na^+]_i$ and $[ATP]_i$ are likely to be influenced by the temperature. While experiments presented here were performed at room temperature (20–22°C), our earlier work has shown that recovery of CA1 pyramidal neurons from global $[Na^+]_i$ transients is accelerated by a factor of ∼2 when increasing the temperature by 10°C (Rose *et al.* 1999; Mondragao *et al.* 2016), indicating that the NKA indeed plays a dominating role in this process. At the same time, mitochondrial generation of ATP will be accelerated at higher temperature, suggesting that both, global $[Na^+]_i$ transients and the accompanying changes in $[ATP]_i$ will be speeded up at physiological temperature (37°C). Recovery from local $[Na^+]_i$ signals, in contrast, is largely driven by diffusion, and consequently, not altered by changing the temperature (Mondragao *et al.* 2016).

Our results strongly suggest that activation of NKA to recover from global $[Na^+]_i$ increases requires, at least temporarily, more ATP than is available and/or produced. As mentioned above, [ATP] will most likely not be rate-limiting for the NKA under the conditions tested here. However, for periods of energy restriction, such as during ischaemia or hypoxia, insufficient ATP availability has been shown to slow down NKA, resulting in a failure of Na^+ extrusion and a rise in $[Na^+]_i$ that aggravates damage by, for example, secondary loading of neurons with protons or Ca^{2+} (Dagani & Erecinska, 1987; Somjen, 2002; Gerkau *et al.* 2017).

In contrast to activity and stimulation patterns that involved global $[Na^+]_i$ elevations, spatially restricted local $[Na^+]_i$ influx as observed upon brief pressure application of glutamate onto dendrites did not evoke a detectable decrease in $[ATP]_i$. A recent study that failed to observe changes in somatic ATP levels in response to electrical activity and Na^+ influx concluded that ATP consumption by the NKA is matched by a direct increase in mitochondrial ATP production (Baeza-Lehnert *et al.* 2019). Earlier work by us and other laboratories, together with the results presented here, provides an alternative and/or additional explanation for the lack of changes in neuronal [ATP] levels despite relevant increases in $[Na^+]_i$ and the efficient recovery thereof.

Peak amplitudes of *local* dendritic $[Na^+]_i$ increases determined in the present study were around 12 mM, which represents a transient doubling of $[Na^+]_i$ (Karus *et al.* 2015; Mondragao *et al.* 2016). In CA1 neurons in acute tissue slices, recovery from a *global* transient increase in $[Na^+]_i$ in the same range (10–15 mM) was dependent on Na^+ extrusion by the NKA (Mondragao *et al.* 2016). Notably, the former study also demonstrated that recovery from locally restricted dendritic $[Na^+]_i$ transients of similar amplitude was not primarily dependent on NKA activity, as it was essentially unaltered during application of ouabain or during energy restriction. Based on these results, it was concluded that the NKA is not involved in the recovery from locally restricted Na^+ influx. Instead the study demonstrated that rapid lateral diffusion of Na^+ from regions with elevated $[Na^+]_i$ to unstimulated parts of the cell is the main mechanism for the recovery of $[Na^+]$ to baseline under these conditions (Mondragao *et al.* 2016). This has also been described for axon initial segments and dendritic spines, where diffusion-driven, intracellular redistribution of Na^+ is the main mechanism for recovery from local Na^+ influx (Fleidervish *et al.* 2010; Miyazaki & Ross, 2017).

The results presented here are in agreement with this latter conclusion. Lateral diffusion of Na^+ does not *per se* involve a consumption of ATP, and we did not detect a change in local [ATP] with local Na^+ transients. In addition to diffusion of Na^+, intracellular diffusion of ATP and/or phosphocreatine, estimated to occur at 500 and 640 $\mu m^2\ s^{-1}$, respectively (de Graaf *et al.* 2000), might counteract a decline in ATP resulting from local activation of the NKA. Combined with a direct stimulation of ATP production (Baeza-Lehnert *et al.* 2019) and with diffusion of ATP itself, diffusion-driven recovery from activity-related $[Na^+]_i$ transients, which does not require direct local ATP consumption, will spread the metabolic burden from activated neuronal microdomains to neighbouring, unstimulated regions.

References

Ainscow EK, Mirshamsi S, Tang T, Ashford ML & Rutter GA (2002). Dynamic imaging of free cytosolic ATP concentration during fuel sensing by rat hypothalamic neurones: evidence for ATP-independent control of ATP-sensitive K^+ channels. *J Physiol* **544**, 429–445.

Akagi K, Nagao T & Urushidani T (1999). Responsiveness of β-escin-permeabilized rabbit gastric gland model: effects of functional peptide fragments. *Am J Physiol* **277**, G736–G744.

Arai S, Kriszt R, Harada K, Looi LS, Matsuda S, Wongso D, Suo S, Ishiura S, Tseng YH, Raghunath M, Ito T, Tsuboi T & Kitaguchi T (2018). RGB-color intensiometric indicators to visualize spatiotemporal dynamics of ATP in single cells. *Angew Chem Int Ed Engl* **57**, 10873–10878.

Baeza-Lehnert F, Saab AS, Gutierrez R, Larenas V, Diaz E, Horn M, Vargas M, Hosli L, Stobart J, Hirrlinger J, Weber B & Barros LF (2019). Non-canonical control of neuronal energy status by the Na^+ pump. *Cell Metab* **29**, 668–680.e4.

Baranauskas G, David Y & Fleidervish IA (2013). Spatial mismatch between the Na^+ flux and spike initiation in axon initial segment. *Proc Natl Acad Sci U S A* **110**, 4051–4056.

Bennay M, Langer J, Meier SD, Kafitz KW & Rose CR (2008). Sodium signals in cerebellar Purkinje neurons and Bergmann glial cells evoked by glutamatergic synaptic transmission. *Glia* **56**, 1138–1149.

Blanco G & Mercer RW (1998). Isozymes of the Na-K-ATPase: heterogeneity in structure, diversity in function. *Am J Physiol* **275**, F633–F650.

Chinopoulos C, Tretter L, Rozsa A & Adam-Vizi V (2000). Exacerbated responses to oxidative stress by an Na^+ load in isolated nerve terminals: the role of ATP depletion and rise of $[Ca^{2+}]_i$. *J Neurosci* **20**, 2094–2103.

Clapham DE (2007). Calcium signaling. *Cell* **131**, 1047–1058.

Close B, Banister K, Baumans V, Bernoth EM, Bromage N, Bunyan J, Erhardt W, Flecknell P, Gregory N, Hackbarth H, Morton D & Warwick C (1997). Recommendations for euthanasia of experimental animals: Part 2. DGXT of the European Commission. *Lab Anim* **31**, 1–32.

Cotter K, Stransky L, McGuire C & Forgac M (2015). Recent Insights into the structure, regulation, and function of the V-ATPases. *Trends Biochem Sci* **40**, 611–622.

Dagani F & Erecinska M (1987). Relationships among ATP synthesis, K^+ gradients, and neurotransmitter amino acid levels in isolated rat brain synaptosomes. *J Neurochem* **49**, 1229–1240.

de Graaf RA, van Kranenburg A & Nicolay K (2000). In vivo ^{31}P-NMR diffusion spectroscopy of ATP and phosphocreatine in rat skeletal muscle. *Biophys J* **78**, 1657–1664.

Dietzel I, Heinemann U, Hofmeier G & Lux HD (1982). Stimulus-induced changes in extracellular Na^+ and Cl^- concentration in relation to changes in the size of the extracellular space. *Exp Brain Res* **46**, 73–84.

Engl E & Attwell D (2015). Non-signalling energy use in the brain. *J Physiol* **593**, 3417–3429.

Erecinska M & Silver IA (1994). Ions and energy in mammalian brain. *Prog Neurobiol* **43**, 37–71.

Fleidervish IA, Lasser-Ross N, Gutnick MJ & Ross WN (2010). Na^+ imaging reveals little difference in action potential-evoked Na^+ influx between axon and soma. *Nat Neurosci* **13**, 852–860.

Fukuda J, Fujita Y & Ohsawa K (1983). ATP content in isolated mammalian nerve cells assayed by a modified luciferin-luciferase method. *J Neurosci Methods* **8**, 295–302.

Gee CE, Ohmert I, Wiegert JS & Oertner TG (2017). Preparation of slice cultures from rodent hippocampus. *Cold Spring Harb Protoc* **2017**, https://doi.org/10.1101/pdb.prot094888.

Gerkau NJ, Rakers C, Durry S, Petzold G & Rose CR (2018). Reverse NCX attenuates cellular sodium loading in metabolically compromised cortex. *Cereb Cortex* **28**, 4264–4280.

Gerkau NJ, Rakers C, Petzold GC & Rose CR (2017). Differential effects of energy deprivation on intracellular sodium homeostasis in neurons and astrocytes. *J Neurosci Res* **95**, 2505–2285.

Haack N, Durry S, Kafitz KW, Chesler M & Rose C (2015). Double-barreled and concentric microelectrodes for measurement of extracellular ion signals in brain tissue. *J Vis Exp*, https://doi.org/10.3791/53058.

Hansen AJ (1985). Effect of anoxia on ion distribution in the brain. *Physiol Rev* **65**, 101–148.

Howarth C, Gleeson P & Attwell D (2012). Updated energy budgets for neural computation in the neocortex and cerebellum. *J Cereb Blood Flow Metab* **32**, 1222–1232.

Imamura H, Huynh Nhat KP, Togawa H, Saito K, Iino R, Kato-Yamada Y, Nagai T & Noji H (2009). Visualization of ATP levels inside single living cells with fluorescence resonance energy transfer-based genetically encoded indicators. *Proc Natl Acad Sci U S A* **106**, 15651–15656.

Jackson JG & Robinson MB (2018). Regulation of mitochondrial dynamics in astrocytes: Mechanisms, consequences, and unknowns. *Glia* **66**, 1213–1234.

Jaffe DB, Johnston D, Lasser-Ross N, Lisman JE, Miyakawa H & Ross WN (1992). The spread of Na^+ spikes determines the pattern of dendritic Ca^{2+} entry into hippocampal neurons. *Nature* **357**, 244–246.

Kaplan JH (2002). Biochemistry of Na,K-ATPase. *Annu Rev Biochem* **71**, 511–535.

Karus C, Mondragao MA, Ziemens D & Rose CR (2015). Astrocytes restrict discharge duration and neuronal sodium loads during recurrent network activity. *Glia* **63**, 936–957.

Knopfel T, Anchisi D, Alojado ME, Tempia F & Strata P (2000). Elevation of intradendritic sodium concentration mediated by synaptic activation of metabotropic glutamate receptors in cerebellar Purkinje cells. *Eur J Neurosci* **12**, 2199–2204.

Konishi M & Watanabe M (1995). Molecular size-dependent leakage of intracellular molecules from frog skeletal muscle fibers permeabilized with β-escin. *Pflugers Arch* **429**, 598–600.

Langer J, Gerkau NJ, Derouiche A, Kleinhans C, Moshrefi-Ravasdjani B, Fredrich M, Kafitz KW, Seifert G, Steinhauser C & Rose CR (2017). Rapid sodium signaling couples glutamate uptake to breakdown of ATP in perivascular astrocyte endfeet. *Glia* **65**, 293–308.

Langer J & Rose CR (2009). Synaptically induced sodium signals in hippocampal astrocytes in situ. *J Physiol* **587**, 5859–5877.

Larsen BR, Stoica A & MacAulay N (2016). Managing brain extracellular K^+ during neuronal activity: The physiological role of the Na^+/K^+-ATPase subunit isoforms. *Front Physiol* **7**, 141.

Lasser-Ross N & Ross WN (1992). Imaging voltage and synaptically activated sodium transients in cerebellar Purkinje cells. *Proc Biol Sci* **247**, 35–39.

Lees GJ (1991). Inhibition of sodium-potassium-ATPase: a potentially ubiquitous mechanism contributing to central nervous system neuropathology. *Brain Res Brain Res Rev* **16**, 283–300.

Leng T, Shi Y, Xiong ZG & Sun D (2014). Proton-sensitive cation channels and ion exchangers in ischemic brain injury: new therapeutic targets for stroke? *Prog Neurobiol* **115**, 189–209.

Lennie P (2003). The cost of cortical computation. *Curr Biol* **13**, 493–497.

Lerchundi R, Kafitz KW, Faerfers M, Beyer F, Huang N & Rose CR (2019*a*). Imaging of intracellular ATP in organotypic tissue slices of the mouse brain using the FRET-based sensor ATeam1.03^{YEMK}. *J Vis Exp* (in press).

Lerchundi R, Kafitz KW, Winkler U, Farfers M, Hirrlinger J & Rose CR (2019*b*). FRET-based imaging of intracellular ATP in organotypic brain slices. *J Neurosci Res* **97**, 933–945.

Lobas MA, Tao R, Nagai J, Kronschlager MT, Borden PM, Marvin JS, Looger LL & Khakh BS (2019). A genetically encoded single-wavelength sensor for imaging cytosolic and cell surface ATP. *Nat Commun* **10**, 711.

Maravall M, Mainen ZF, Sabatini BL & Svoboda K (2000). Estimating intracellular calcium concentrations and buffering without wavelength ratioing. *Biophys J* **78**, 2655–2667.

Martinez-Francois JR, Fernandez-Aguera MC, Nathwani N, Lahmann C, Burnham VL, Danial NN & Yellen G (2018). BAD and K_{ATP} channels regulate neuron excitability and epileptiform activity. *Elife* **7**, e32721.

Meier SD, Kovalchuk Y & Rose CR (2006). Properties of the new fluorescent Na^+ indicator CoroNa Green: comparison with SBFI and confocal Na^+ imaging. *J Neurosci Methods* **155**, 251–259.

Mendelsohn BA, Bennett NK, Darch MA, Yu K, Nguyen MK, Pucciarelli D, Nelson M, Horlbeck MA, Gilbert LA, Hyun W, Kampmann M, Nakamura JL & Nakamura K (2018). A high-throughput screen of real-time ATP levels in individual cells reveals mechanisms of energy failure. *PLoS Biol* **16**, e2004624.

Misgeld T & Schwarz TL (2017). Mitostasis in neurons: maintaining mitochondria in an extended cellular architecture. *Neuron* **96**, 651–666.

Miyazaki K & Ross WN (2017). Sodium dynamics in pyramidal neuron dendritic spines: synaptically evoked entry predominantly through AMPA receptors and removal by diffusion. *J Neurosci* **37**, 9964–9976.

Mollajew R, Toloe J & Mironov SL (2013). Single KATP channel opening in response to stimulation of AMPA/kainate receptors is mediated by Na^+ accumulation and submembrane ATP and ADP changes. *J Physiol* **591**, 2593–2609.

Mondragao MA, Schmidt H, Kleinhans C, Langer J, Kafitz KW & Rose CR (2016). Extrusion versus diffusion: mechanisms for recovery from sodium loads in mouse CA1 pyramidal neurons. *J Physiol* **594**, 5507–5527.

Nakano M, Imamura H, Nagai T & Noji H (2011). Ca^{2+} regulation of mitochondrial ATP synthesis visualized at the single cell level. *ACS Chem Biol* **6**, 709–715.

Ona-Jodar T, Gerkau NJ, Sara Aghvami S, Rose CR & Egger V (2017). Two-photon Na^+ imaging reports somatically evoked action potentials in rat olfactory bulb mitral and granule cell neurites. *Front Cell Neurosci* **11**, 50.

Pathak D, Shields LY, Mendelsohn BA, Haddad D, Lin W, Gerencser AA, Kim H, Brand MD, Edwards RH & Nakamura K (2015). The role of mitochondrially derived ATP in synaptic vesicle recycling. *J Biol Chem* **290**, 22325–22336.

Proks P & Ashcroft FM (2009). Modeling K_{ATP} channel gating and its regulation. *Prog Biophys Mol Biol* **99**, 7–19.

Rangaraju V, Calloway N & Ryan TA (2014). Activity-driven local ATP synthesis is required for synaptic function. *Cell* **156**, 825–835.

Rose CR (2002). Na^+ signals at central synapses. *Neuroscientist* **8**, 532–539.

Rose CR & Konnerth A (2001). NMDA receptor-mediated Na^+ signals in spines and dendrites. *J Neurosci* **21**, 4207–4214.

Rose CR, Kovalchuk Y, Eilers J & Konnerth A (1999). Two-photon Na^+ imaging in spines and fine dendrites of central neurons. *Pflugers Arch* **439**, 201–207.

Rueda CB, Traba J, Amigo I, Llorente-Folch I, Gonzalez-Sanchez P, Pardo B, Esteban JA, del Arco A & Satrustegui J (2015). Mitochondrial ATP-Mg/Pi carrier SCaMC-3/Slc25a23 counteracts PARP-1-dependent fall in mitochondrial ATP caused by excitotoxic insults in neurons. *J Neurosci* **35**, 3566–3581.

Sheldon C, Cheng YM & Church J (2004). Concurrent measurements of the free cytosolic concentrations of H^+ and Na^+ ions with fluorescent indicators. *Pflugers Arch* **449**, 307–318.

Sobieski C, Fitzpatrick MJ & Mennerick SJ (2017). Differential presynaptic ATP supply for basal and high-demand transmission. *J Neurosci* **37**, 1888–1899.

Somjen GG (2002). Ion regulation in the brain: implications for pathophysiology. *Neuroscientist* **8**, 254–267.

Somjen GG (2004). *Ions in the Brain: Normal Function, Seizures, and Stroke*. Oxford University Press, New York.

Stoppini L, Buchs PA & Muller D (1991). A simple method for organotypic cultures of nervous tissue. *J Neurosci Methods* **37**, 173–182.

Suzuki R, Hotta K & Oka K (2018). Transitional correlation between inner-membrane potential and ATP levels of neuronal mitochondria. *Sci Rep* **8**, 2993.

Sweadner K (1995). Sodium, potassium-adenosine triphosphatase and its isoforms. In *Neuroglia*, ed. Kettenmann HRB, pp. 259–272. Oxford University Press, Oxford, New York.

Tanner GR, Lutas A, Martinez-Francois JR & Yellen G (2011). Single K_{ATP} channel opening in response to action potential firing in mouse dentate granule neurons. *J Neurosci* **31**, 8689–8696.

Tantama M, Hung YP & Yellen G (2012). Optogenetic reporters: Fluorescent protein-based genetically encoded indicators of signaling and metabolism in the brain. *Prog Brain Res* **196**, 235–263.

Tantama M, Martinez-Francois JR, Mongeon R & Yellen G (2013). Imaging energy status in live cells with a fluorescent biosensor of the intracellular ATP-to-ADP ratio. *Nat Commun* **4**, 2550.

Therien AG & Blostein R (2000). Mechanisms of sodium pump regulation. *Am J Physiol Cell Physiol* **279**, C541–C566.

Thompson SM & Prince DA (1986). Activation of electrogenic sodium pump in hippocampal CA1 neurons following glutamate-induced depolarization. *J Neurophysiol* **56**, 507–522.

Toloe J, Mollajew R, Kugler S & Mironov SL (2014). Metabolic differences in hippocampal 'Rett' neurons revealed by ATP imaging. *Mol Cell Neurosci* **59**, 47–56.

Trevisiol A, Saab AS, Winkler U, Marx G, Imamura H, Mobius W, Kusch K, Nave KA & Hirrlinger J (2017). Monitoring ATP dynamics in electrically active white matter tracts. *Elife* **6**, e24241.

Winkler U, Seim P, Enzbrenner Y, Kohler S, Sicker M & Hirrlinger J (2017). Activity-dependent modulation of intracellular ATP in cultured cortical astrocytes. *J Neurosci Res* **95**, 2172–2181.

Yaginuma H, Kawai S, Tabata KV, Tomiyama K, Kakizuka A, Komatsuzaki T, Noji H & Imamura H (2014). Diversity in ATP concentrations in a single bacterial cell population revealed by quantitative single-cell imaging. *Sci Rep* **4**, 6522.

Yuste R, Majewska A & Holthoff K (2000). From form to function: calcium compartmentalization in dendritic spines. *Nat Neurosci* **3**, 653–659.

Zanotto L & Heinemann U (1983). Aspartate and glutamate induced reductions in extracellular free calcium and sodium concentration in area CA1 of 'in vitro' hippocampal slices of rats. *Neurosci Lett* **35**, 79–84.

Additional information

Competing interests

The authors declare no conflict of interest and no competing financial interest.

Author contributions

All authors take responsibility for the integrity of the data and the accuracy of the data analysis. Study concept and design: N.J.G. and C.R.R. Acquisition of data: N.J.G., R.L., J.S.E.N., M.L. and J.M. Analysis and interpretation of data: N.J.G., R.L. and C.R.R. Figure preparation: N.J.G. and C.R.R. Drafting of the manuscript: N.J.G. and C.R.R. Final editing of manuscript: N.J.G., R.L., J.S.E.N., J.M., J.H. and C.R.R. Funding acquisition: J.H. and C.R.R. All authors have read and approved the final version of this manuscript and agree to be accountable for all aspects of the work in ensuring that questions related to the accuracy or integrity of any part of the work are appropriately investigated and resolved. All persons designated as authors qualify for authorship, and all those who qualify for authorship are listed.

Funding

This work was supported by the Deutsche Forschungsgemeinschaft (FOR 2795: Ro2327/13-1; Hi1414/6-1).

Acknowledgements

We thank Claudia Roderigo and Simone Durry (Institute of Neurobiology) for expert technical assistance. We also thank Andrea Trevisiol at the Max-Planck-Institute for Experimental Medicine, Göttingen, Germany, for help with the ATP reporter animals.